RSC Advances

PAPER

View Article Online
View Journal | View Issue

Cite this: *RSC Adv.*, 2018, **8**, 18388

The pH dependent reactions of graphene oxide with small molecule thiols†

Al de Leon,[a] Michael Mellon,[b] Joey Mangadlao,[c] Rigoberto Advincula[d] and Emily Pentzer *[a]

Graphene oxide (GO) is a heterogenous 2D carbon-based material composed of sp^2 and sp^3 hybridized carbon atoms and oxygen containing functionalities, *i.e.*, alcohols and epoxides. Thus, the chemical reactivity of GO is complex and both complimentary and contrasting to the reactivity of corresponding small molecules (*e.g.*, tertiary alcohols, epoxides, and alkenes). Understanding the reactivity of GO under different conditions and with different reagents will ensure the chemical composition can be controlled and thus electronic and optical properties dictated, and solubility tuned for desired applications. Reaction of GO nanosheets towards a variety of reagents has been reported, however controlling the reaction pathway of GO nanosheets with a single nucleophile by simple alternation of the reaction medium has not been realized. This ability to tune the reaction by modification of solution pH, for example, would aid in understanding the reactivity of GO. Herein, we report that GO undergoes two distinct reaction pathways with ethane thiol depending on the pH of the reaction media: under aprotic basic conditions GO nanosheets undergo functionalization with minimal reduction, and under superacidic conditions GO nanosheets are reduced with no functionalization.

Received 17th April 2018
Accepted 11th May 2018

DOI: 10.1039/c8ra03300e

rsc.li/rsc-advances

1. Introduction

Graphene oxide (GO) nanosheets are composed of a 2D framework of carbon atoms decorated with oxygen functionalities. This nanomaterial has garnered much interest for a wide variety of applications, from energy harvesting and storage to biomedical devices to sensors.[1–6] The applications of GO are dependent on its chemical nature, *i.e.*, extent of oxidation, nanosheet diameter, and functionalization.[7–10] Most commonly, GO is prepared by the chemical oxidation of graphite using the strong oxidizing agent potassium permanganate ($KMnO_4$) in a strongly acidic solution (H_2SO_4).[11,12] The generally accepted chemical model of GO has oxygen functionalities such as epoxides and alcohols on the basal plane and carboxylic acids on the edges of the nanosheets, as proposed in the Lerf–Klinowski model.[13–17] Aggregated GO nanosheets (commonly called graphite oxide) are exfoliated into individual nanosheets suspended in solution, and then reduced and/or functionalized using a number of reagents, with choice depending on the properties required for a given application.[18–20] Reduced GO has been used in transparent and flexible electronic devices and sensors, while chemically functionalized GO has been used as filler in polymer composites, surfactant in Pickering emulsions, and a component in hybridized materials.[14,15] This method of graphite → GO → functionalized and/or reduced GO is widely used by researchers across different fields.[21–24]

The chemical composition of GO can vary by the preparation and processing methods used,[13,25–27] and a distribution of nanosheets will be presented with variations and heterogeneities observed between nanosheets and across the surface of a single nanosheet. Both functionalization and reduction of GO are impacted and complicated by the heterogeneity of the material, as well as by the interconnectivity of the functional groups. For example, treatment of GO with strong acid protonates double bonds or alcohols to produce carbocations that can delocalize across neighboring alkene units and hydroxyl groups (*i.e.*, conjugation and anomeric effect), and thus lead to unexpected functionalization. Moreover, the complex nature of GO means that it can be reduced using metal hydrides and borohydrides, distinct from small molecules bearing alcohol, epoxide, and alkene functionalities.[26,28–30] Whereas fundamental reactions such as ring opening of epoxides and esterification of alcohols and carboxylic acids can be used to modify GO,[10,19,27,31–33] functionalization is typically accompanied by reduction of the GO nanosheets, and the two reaction pathways cannot be disentangled and predictable

[a]*Department of Chemistry, Case Western Reserve University, 10900 Euclid Ave. 46106, USA*

[b]*Department of Chemistry, Kentucky State University, 400 East Main St. Frankfort, KY 40601, USA*

[c]*Department of Radiology, Case Western Reserve University, 10900 Euclid Ave. 46106, USA*

[d]*Department of Macromolecular Science and Engineering, Case Western Reserve University, 10900 Euclid Ave. 46106, USA. E-mail: ebp24@case.edu*

† Electronic supplementary information (ESI) available. See DOI: 10.1039/c8ra03300e

reactivity can be obscured. An inherent reactivity of GO nanosheets also exists, with net disproportionation reactions occurring when the material is stored in water that leads to smaller diameter nanosheets, as established by Tour *et al.*[34] Thus, understanding how reaction conditions impact the functionalization and reduction of GO is necessary to perform reactions in a controlled and repeatable fashion.

Herein, we report the reaction of GO nanosheets with a primary thiol under acidic and basic conditions. Thiols have not been used to functionalize GO, likely due to the multifaceted reactivity of these molecules as bases, acids, nucleophiles, and reducing agents.[35–38] We illustrate the dependence of the mode of reactivity–reduction *versus* functionalization on the pH of the solution. In the presence of ethane thiol (EtSH) in a superacid solution (10 : 1 vol : vol acetic acid : sulfuric acid), GO is reduced with little-to-no functionalization observed; in contrast, in the presence of EtSH in a basic solution (*N*,*N*-diisopropyl methylamine in DMSO), GO is functionalized but not significantly reduced (Scheme 1). X-ray photoelectron spectroscopy (XPS) is used to demonstrate changes in the chemical composition of the nanosheets upon reaction, while solubility, Raman spectroscopy, X-ray diffraction (XRD), thermogravimetric analysis (TGA), and four-point probe conductivity measurements are used to differentiate the materials. Reaction of EtSH under acidic and neutral aprotic solvent neither reduced nor functionalized graphene oxide, thus illustrating the importance of solution pH.

2. Experimental

2.1. Materials and instrumentations

Graphite flakes, potassium permanganate, sulfuric acid, aqueous hydrogen peroxide solution (30 wt%), isopropanol, acetic acid, sulfuric acid, *N*,*N*-diisopropylethylamine, and ethane thiol were purchased from Sigma-Aldrich and were used as received. Tapping mode atomic fore microscopy (AFM) was performed in a NX-10 Park system. FTIR spectra were collected from a Cary 600 by Agilent Technologies in ATR mode. X-Ray photoelectron spectroscopy data (survey and high-resolution scans) were collected using PHI Versaprobe 5000 X-ray photoelectron spectrometer with Al Kα radiation and was referenced to internal SiO_2. Raman Spectra were acquired using a Jasco Analytic Instruments NRS-4100 with 532 nm excitation. 2D X-ray diffraction experiment was performed using Bruker Discover D8 X-ray diffractometer, which has a monochromated X-ray source (normally used with a Co K-alpha X-ray tube), configured in point focus mode. Thermogravimetric analysis was performed in a TGA 2050 system by TA Instruments set at 10 °C min^{-1}. UV-Vis spectra were collected using Agilent Cary 5000 UV-Vis-NIR in a quartz cuvette. Fluorescence studies were performed using Agilent Cary Eclipse fluorescence spectrophotometer. Sheet resistances were measured using EDTM R-Chek four-point probe.

2.2. Preparation of graphene oxide

Graphene oxide was prepared by dispersing 6 g of graphite flakes in 800 mL of sulfuric acid in a beaker equipped with magnetic stirring at room temperature under ambient conditions. 6 g of potassium permanganate was added after graphite was completely dispersed. The dispersion was stirred for 1 day, after which another 6 g of potassium permanganate was added. This was repeated two more times (24 g of $KMnO_4$ total added). 24 h after the addition of the 4th batch of potassium permanganate, the reaction mixture was quenched in ice-water. An aqueous hydrogen peroxide solution (30%) was added dropwise while stirring until the pink color of the excess potassium permanganate disappeared. The GO dispersion was centrifuged to separate the acidic supernatant. The pellet was then washed at least seven times with isopropyl alcohol by centrifugation until the supernatant was neutral, as determined by litmus paper. The isolated GO was dried under reduced pressure until the weight remained constant.

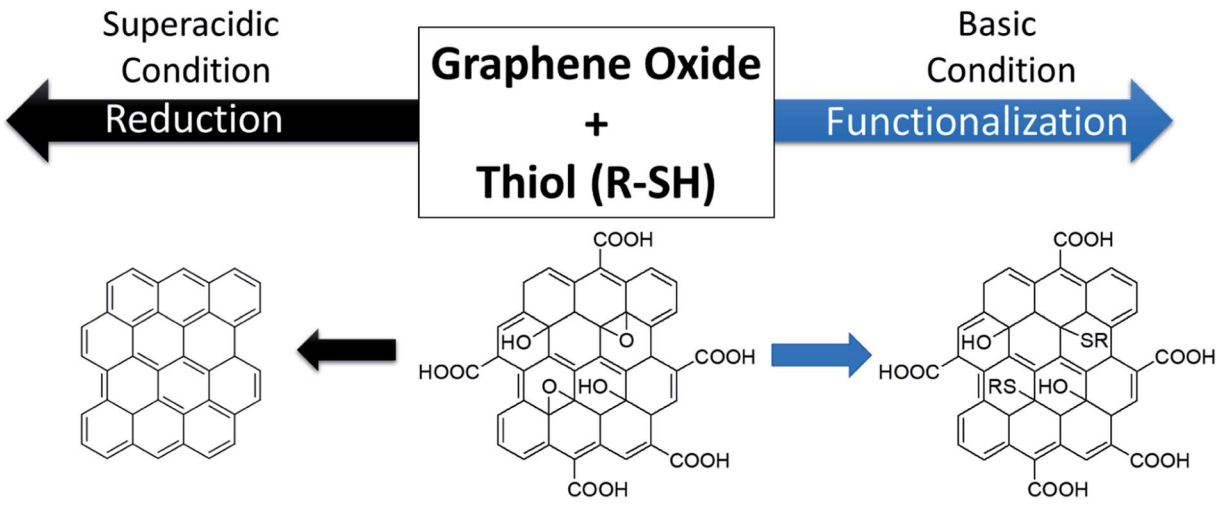

Scheme 1 Overview of the work reported herein: in the presence of ethane thiol (EtSH), graphene oxide (GO) nanosheets can be reduced in a superacidic solution, or functionalized in a basic solution.

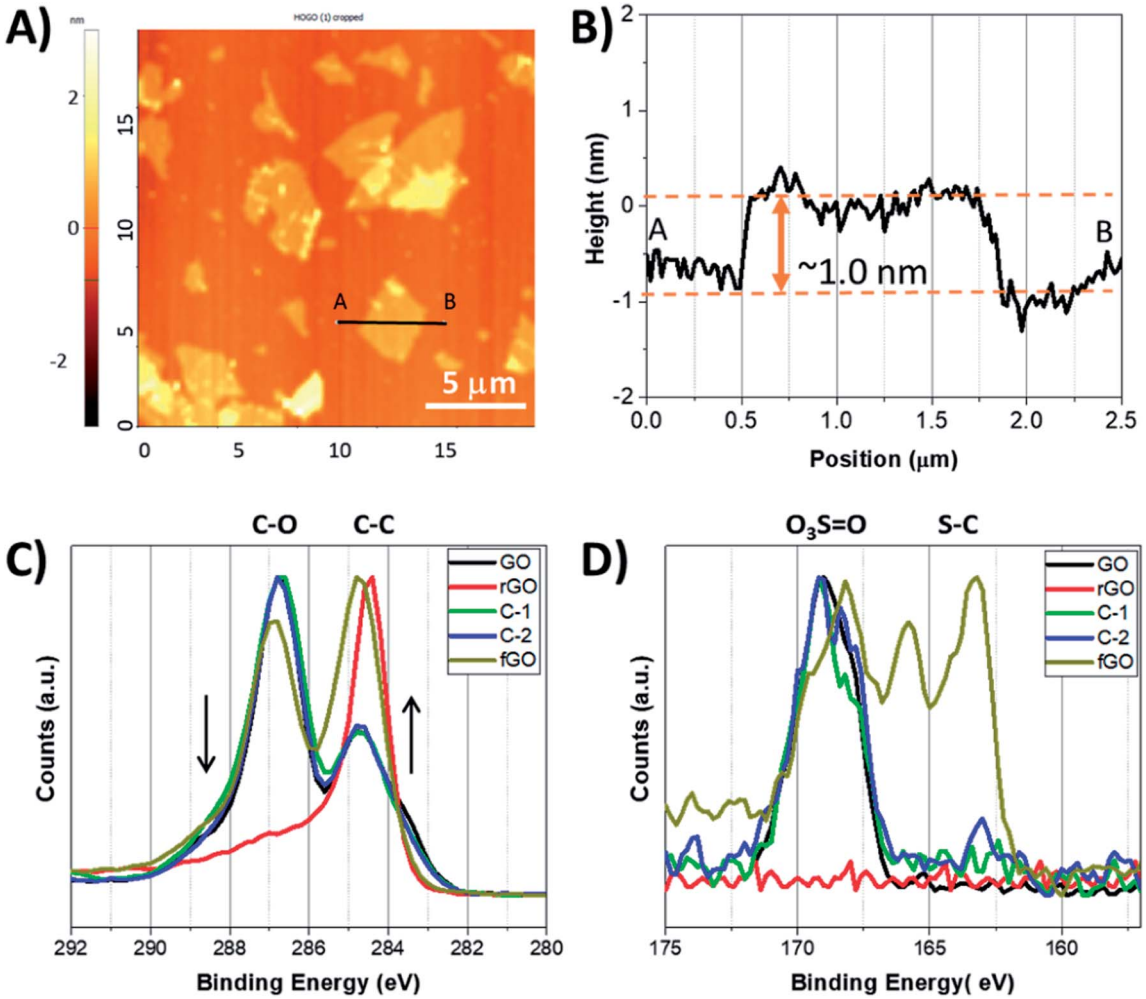

Fig. 1 A) AFM image of GO nanosheets prepared by drop-casting an aqueous dispersion onto mica substrate; (B) Line profile of GO nanosheet indicated in A; (C) C 1s high resolution XPS scan; (D) S 2p3/2 high resolution XPS scan. GO (black trace), rGO (red trace), fGO (olive trace), C-1 (green), and C-2 (blue).

2.3. Preparation of fGO and rGO

Preparation of fGO involved the dispersion of 50 mg of GO in 50 mL DMSO with 2 vol% *N*,*N*-diisopropyl ethylamine. 2 mL of ethane thiol was then added and the dispersion was allowed to stir for 24 hours under ambient conditions. The resulting fGO was washed with methanol by centrifugation four times and with acetone once. The solid product was collected and dried under reduced pressure. Preparation of rGO was achieved by dispersion of 50 mg of GO in a mixture of 45 mL acetic acid and 5 mL of concentrated sulfuric acid. 2 mL of ethane thiol was then added and the dispersion was allowed to stir for 24 hours. The resulting rGO was washed with methanol by centrifugation four times and with acetone once. The solid product was collected and dried under reduced pressure. Control experiments were performed similarly but using 50 mL DMSO with 2 mL of concentrated sulfuric acid (for C-1) and using 50 mL DMSO (for C-2).

3. Results and discussion

GO was prepared by extended oxidation of graphite in sulfuric acid, by adding one mass equivalent of potassium permanganate per day for four days.[34] These extended oxidative conditions ensure that GO contains alcohol, epoxide, and carbonyl-containing functional groups, giving a C : O ratio of 1.54 : 1. By washing GO in a polar protic solvent (*i.e.*, not water), sulfates are covalently bound to the nanosheet surface, lending long term stability to the material when stored in the solid state by preventing disadvantageous reactions (*i.e.*, disproportionation).[34] GO nanosheets were easily dispersed in water using mild sonication, and individual nanosheets were obtained, as seen in Fig. 1A and B; exfoliated nanosheets were microns in diameter and had thickness of ~1 nm, as determined by atomic force microscopy (AFM), consistent with single nanosheets.[39–41] GO nanosheets were suspended in either a mixture of acetic acid and sulfuric acid (10 : 1 vol : vol, termed superacid) or

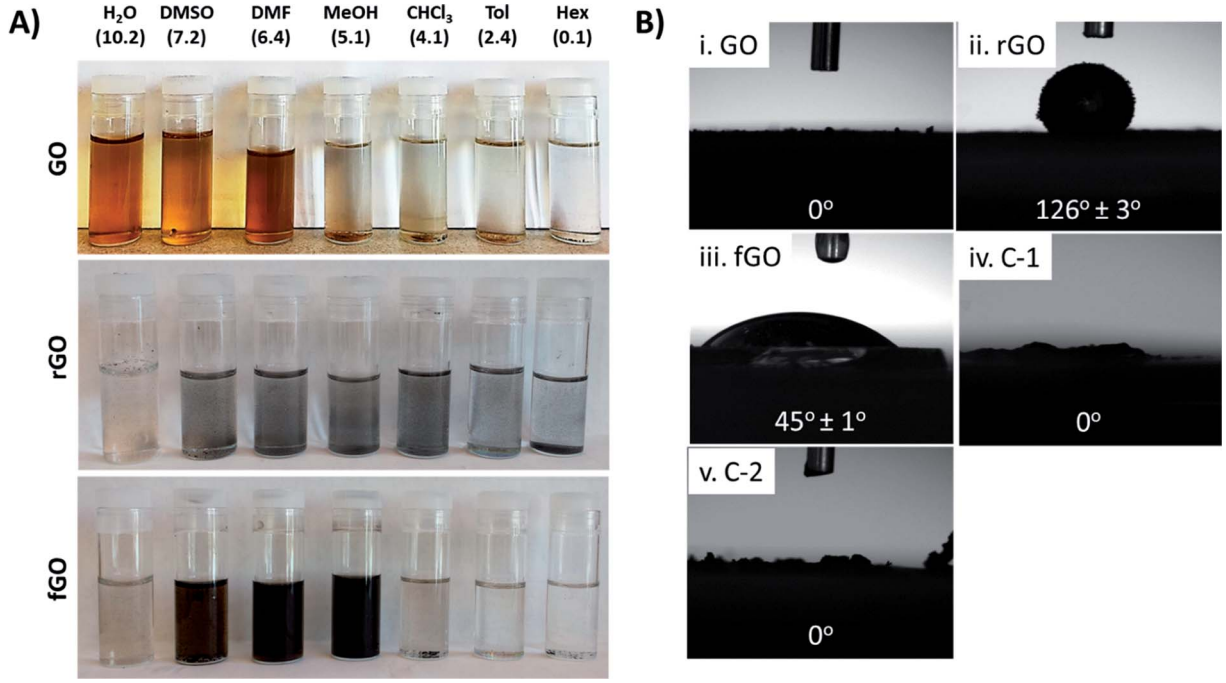

Fig. 2 (A) Solubility profiles of GO (top), rGO (middle), and fGO (bottom) in solvents of different polarity after 24 hours (numbers under solvent refer to dielectric constants); (B) water contact angles of drop cast films of GO (i), rGO (ii), fGO (iii), C-1 (iv), and C-2 (v).

basic DMSO (2 vol% *N*,*N*-diisopropyl ethylamine, termed basic solution), then ethane thiol (EtSH) was added. In the super-acidic solution, GO was reduced and in basic solution GO was functionalized, and the products are referred to as rGO and fGO, respectively. To verify that the combination of thiol and pH are responsible for the chemical transformations observed, a control reaction was performed with EtSH in acidic DMSO (2 vol% sulfuric acid, C-1) and EtSH in neutral DMSO (C-2).

To examine how reaction conditions impacted the chemical composition of the products, X-ray photoelectron spectroscopy (XPS) was used.[42–44] Survey scans of fGO, rGO, C-1, and C-2 show carbon and oxygen are the major constituent atoms, as expected (Fig. S1†), with GO having 1.54 graphitic carbon atoms per oxygen (Fig. S1 and Table S1†). In contrast, the C : O ratio of rGO substantially increased to 5.34 : 1, and minimally changed for fGO, C-1, or C-2 (1.73 : 1, 1.75 : 1, and 1.78 : 1, respectively). The chemical composition can be better understood from high resolution C 1s and S 2p3/2 spectra (Fig. 1C and D). In high resolution C 1s spectra, a peak at 284.4 eV is assigned to C–C, C=C, and C–H bonds, and peak(s) above 285.0 eV correspond to oxidized carbon, *e.g.*.C–O and C=O (Fig. S2a–e†).[44] As seen in Fig. 1C, GO has a higher contribution from C–O/C=O than C–C/C=C, and this distribution was unaltered for C-1 and C-2. Only a slight decrease in the contribution of oxygenated carbon is observed for fGO, while the spectrum for rGO shows C–C/C=C is the dominant species, as typical for highly reduced GO. Of note, the ratio of oxygenated to non-oxygenated carbon atoms does not change for GO treated with only superacid (*i.e.*, without R–SH) and the C 1s spectrum is unchanged from that of GO (Fig. S2†). The high-resolution S 2p3/2 spectra can also be used

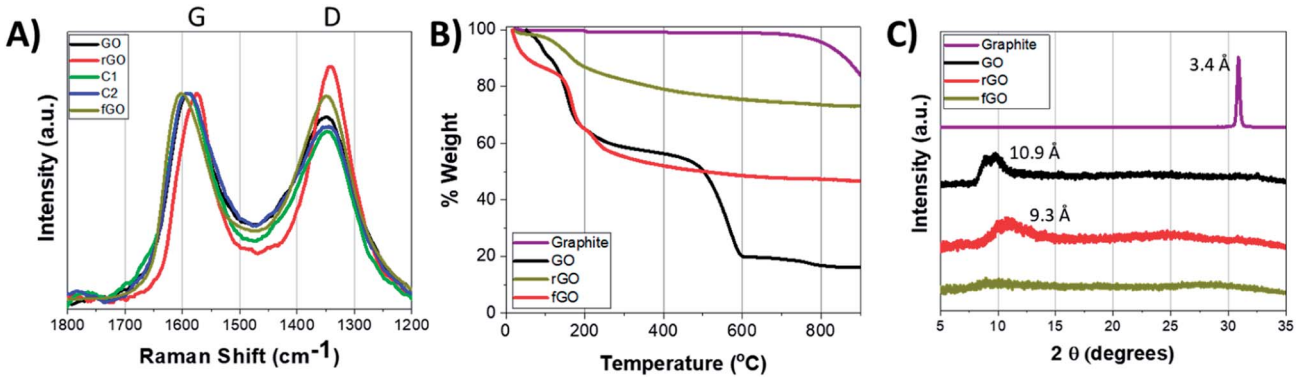

Fig. 3 (A) Raman spectra; (B) XRD spectra; (C) TGA weight loss profiles of: GO (black traces), rGO (red traces), fGO (olive traces), C-1 (green traces), and C-2 (blue traces).

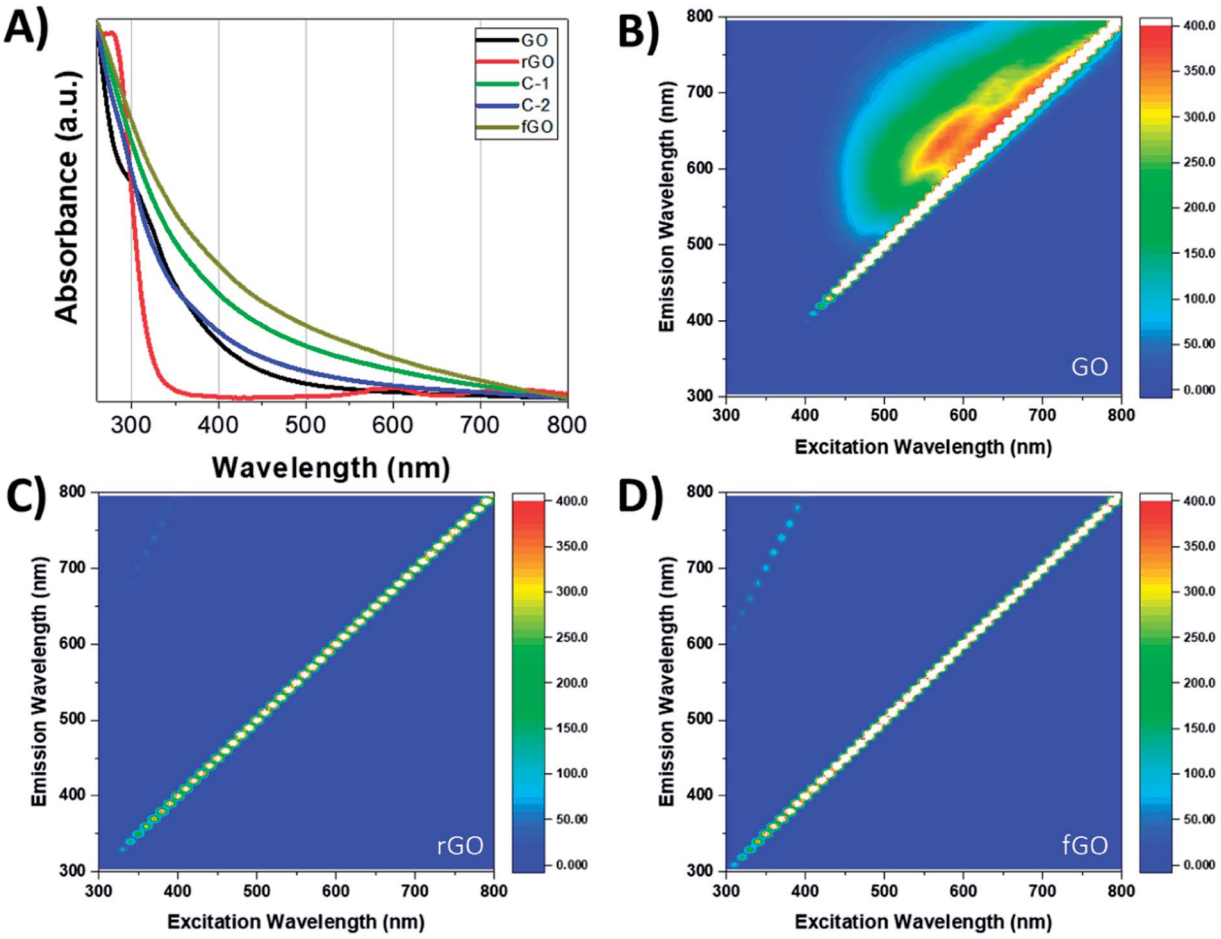

Fig. 4 (A) UV-Vis spectra of GO, rGO, fGO, C-1, and C-2 suspended in DMSO; 2D fluorescence spectra of (B) GO; (C) rGO; and (D) fGO.

to understand the functionality of the materials; as seen in Fig. 1D, the S 2p3/2 spectrum of GO reveals covalently bound sulfates ($O_3S{=}O$) by the peak at 168.2 eV, and the spectra are similar for C-1 and C-2.[45,46] In contrast, the S 2p3/2 XPS spectrum of fGO shows a peak at 163.2 eV and indicates the presence of S–C bonds, and that sulfate peaks remain (168.2 eV); the peak between the C–S and $O_3S{=}O$ bonds at 165.5 eV suggests that sulfinyl (S=O)-based functional groups are also present, potentially by the partial reduction of sulfonates. These data also indicate that for fGO, one sulfur atom is incorporated for every 55 graphitic carbon atoms (Table S1†). On the other hand, the S 2p3/2 spectrum of rGO was featureless, indicating neither $O_3S{=}O$ nor S–C and that the nanosheets were not modified. Similar reactions performed in basic aqueous solution showed no incorporation of thiol, but only significant reduction of the nanosheets (Fig. S3†).

By reducing and/or functionalizing GO, its solubility can be controlled, which in turn dictates the applications and the composites that can be prepared.[20,47,48] Fig. 2 demonstrates the distinct difference in the solubility profiles of GO, rGO, and fGO. GO is easily dispersed in polar solvents such as water (H_2O), dimethyl sulfoxide (DMSO), and *N*,*N*-dimethylformamide (DMF) and remains dispersed after 24 hours; however, after 24 hours, GO precipitates from less polar solvents such chloroform ($CHCl_3$) and methanol (MeOH), and GO cannot be dispersed in nonpolar solvents such as toluene (Tol) and hexanes (Hex). The middle panel of Fig. 2A shows that rGO precipitates from all solvents after 24 hours, which can be attributed to strong van der Waals interactions between nanosheets (*i.e.*, π–π stacking).[21,32] Alternatively, as shown in the bottom panel of Fig. 2A, fGO is dispersible in polar organic solvents such as DMSO, DMF, and MeOH, but is not dispersible in water. The dark color of the solutions indicates that the nanosheets are slightly reduced (see above), and the solubility profile indicates that attachment of EtSH shifts the polarity of the nanosheets; however, the short alkyl chain (ethyl) of the thiol is not sufficient to render fGO dispersible in more nonpolar solvents such as $CHCl_3$, Tol, and Hex. Fig. 2B shows the water contact angle for drop cast films of GO, rGO, fGO, C-1, and C-2; change in the polarity of nanosheets upon reduction and functionalization clearly impacts their interactions with water. Fig. 2Bi reveals that films of GO are hydrophilic and water spontaneously spreads across the surface, giving contact angle of 0°. In contrast, a film of rGO is substantially more hydrophobic, as expected, giving a water contact angle of 126° ± 3°, while a film of fGO has an intermediate value of 45° ± 1°. This

Table 1 Chemical composition, as determined by XPS, and sheet resistance of GO, rGO, and fGO. Averages and standard deviations of sheet resistance are based on 5 measurements

Sample	% Graphitic C	% O	% S (as C–S)	Graphitic C : O	Thiol : Graphitic C	Sheet resistance ($k\Omega\ sq^{-1}$)
GO	60.6	39.4	0	1.54 : 1	0	529 ± 10
rGO	84.3	15.7	0	5 : 37 : 1	0	127 ± 7.3
fGO	61.3	35.4	1.1	1 : 73 : 1	1 : 55	459 ± 8.3

data indicates that rGO and fGO are more hydrophobic than GO, although the water contact angles may be impacted by surface roughness, and thus nanosheet–nanosheet interactions (*i.e.*, a rougher film leads to larger contact angle).[49] Films of the control samples C-1 and C-2 had contact angles consistent with GO (0°), and again support that insignificant reduction or functionalization occurred.

To further understand differences in the properties of GO, fGO, and rGO, Raman spectroscopy, X-ray diffraction analysis (XRD), and thermogravimetric analysis (TGA) were performed. In Raman spectroscopy, chemical and structural changes of GO are characterized using two peaks: the G-band (1590 cm^{-1}) corresponding to the primary in-plane vibrational mode of the sp^2 carbon atoms, and the D-band (1350 cm^{-1}) corresponding to disorder of graphitic domains, either on nanosheet edges or internal atomic defects.[23,50–52] As can be seen in the Raman spectra of Fig. 3A and Table S1,† rGO has an increase in the D band intensity relative to the G band intensity compared to GO, and this can be attributed to restoration of small graphitic domains upon reduction. In contrast, fGO shows only a slight increase in the D band intensity relative to the G band intensity, which likely corresponds to increase in disorder due to the functionalization. For C-1 and C-2, changes in the ratio of D and G band intensities are nominal. TGA weight loss profiles were then collected to understand the functionalization and reduction, and compared to graphite (Fig. 3B).[20,43,47,53] Graphite only showed significant weight loss when heating above 900 °C; however, GO showed a multi-step weight loss profile: ~8% loss after heating to 100 °C due to the removal of adsorbed water; ~27% loss upon heating to 200 °C due to the loss of labile oxygen-containing functional groups; ~40% loss upon heating to 600 °C due to pyrolysis of the carbon skeleton; and ~3% loss upon heating to 800 °C due to detachment of covalently bound sulfates.[34] The weight loss profile of fGO is similar to that of GO but with less contribution from oxygen- and sulfate-containing functional groups; in contrast, the weight loss profile of rGO is more similar to graphite, but with loss of adsorbed water. XRD was then used to identify nanosheet interactions and stacking (Fig. 3C).[28,54–56] Pure graphite shows a peak at 30.9° corresponding to interlayer spacing of 3.4 Å and can be attributed to π–π stacking, whereas GO nanosheets show increased interlayer spacing of 10.9 Å (peak at 9.7°), which indicates the nanosheets stack, but not as tightly.[13] rGO nanosheets have an intermediate interlayer distance to that of graphite and GO, with a peak at 12.5° corresponding to a distance of 9.2 Å, whereas the spectrum of fGO is featureless, with no peaks observed from 5° to 35°. These data indicate that removal of oxygen functionalities facilitate the nanosheet–nanosheet stacking of rGO but residual functionalities prevent the tight stacking of graphite; further, fGO nanosheets do not have strong nanosheet–nanosheet interactions, likely due to steric considerations of the ethyl group which cause disorder.

The optoelectronic properties of GO and its reduced and functionalized analogues are relatively understudied, but these properties are vital to various applications.[29,34,41] Fig. 4 shows the UV-Vis absorption and excitation–emission profiles of GO, rGO, and fGO. The UV-Vis spectrum of GO in H_2O has a peak at 229 nm attributed to ketones, dienes, and π–π transitions of C=C, and is accompanied by a shoulder at 304 nm, attributed to the *n*–π transition of C=O (Fig. S4†); alternatively, the UV-Vis spectrum of GO in DMSO (black trace) shows a similar shoulder at 304 nm, but the peak at 229 nm is not apparent due to absorption of DMSO at <268 nm. The maximum absorption of rGO is a redshifted compared to GO, with a peak at 276 nm, which can be attributed to the restoration of the conjugated structure, and the shoulder at 304 nm disappears due to loss of carbonyl functionalities.[32] Likewise, the absorption profile of fGO shows the disappearance of the shoulder, but an increase in absorption over the entire range evaluated. The emission of GO against excitation wavelength is shown in Fig. 4B and reveals broad emission; in contrast, neither rGO and fGO have emission over the entire range of excitation (Fig. 4C and D). As fluorescence of GO is attributed to electronic transitions of graphitic domains at the boundary of the oxidized regions,[57,58] in both rGO and fGO this mechanism must be perturbed or suppressed.

For many applications, GO nanosheets must be electrically conductive, and this is most typically achieved by not only removal of oxygen functional groups, but also reinstatement of conjugated domains. The elemental composition and four-point probe resistivity measurements of drop cast films of GO, rGO, and fGO are shown in Table 1.[20,59,60] These data show that the material with the highest C : O ratio (rGO) has the lowest resistivity, and thus highest conductivity. The sheet resistance of films of GO was $529 \pm 10\ k\Omega\ sq^{-1}$, which is higher than values previously reported in the literature,[61] and likely due to the extensive oxidation conditions used for the present studied that incorporated more oxygen functionalities (*i.e.*, fewer conjugated domains). Films of fGO nanosheets, which underwent functionalization but not substantial reduction, had a sheet resistance of $459 \pm 8.3\ k\Omega\ sq^{-1}$, only slightly lower than that of GO.

In contrast, films of rGO had a substantially lower sheet resistance of 127 ± 7.3 kΩ sq^{-1}.

4. Conclusion

Herein we reported the selective reduction or functionalization of graphene oxide nanosheets with a thiol by varying the pH of the reaction medium. The characterization data presented above show that the combination of EtSH and solution pH are responsible for the nature of the chemical modification of GO nanosheets, either functionalization or reduction. The GO nanosheets used as the starting material in these studies showed typical solubility profile, wettability, C : O ratio, thermal stability, and optoelectronic and electrical properties, and the materials produced after reaction with EtSH in superacid or basic DMSO are distinctly different from the starting material and each other. Functionalization with minimal reduction was observed by treatment of GO with EtSH in basic aprotic solvent and reduction of GO with no functionalization was observed upon treatment of GO with EtSH was in superacidic solvent. The modified materials were characterized by high resolution XPS scans, UV-Vis, and Raman spectroscopy were all used to characterized the modified materials. Reduction and functionalization by EtSH resulted in a change in interlayer distance between GO sheets as shown by XRD and drastic change in polarity verified by dispersability and contact angle measurements. Electrical conductivity was also shown to be restored for rGO but not as much for fGO. These results illustrate that not only do reagents impact the reduction and/or functionalize GO nanosheets, but other solution parameters, namely pH, play a concurrent role in dictating product formation. The different mechanist pathways are currently illusive, and likely include both traditional organic reactions (*e.g.*, protonation/deprotonation), as well as electron transfer reactions (*e.g.*, formation and cleavage of disulfides). Ongoing work focuses on understanding these reaction pathways and expanding the thiols that can be used to functionalize GO, including other small molecules and thiol-containing polymers.

Conflicts of interest

There are no conflicts to declare.

Acknowledgements

The authors thank CWRU College of Arts and Sciences for financial support and Jasco Analytical Instruments for Raman spectroscopy. The authors thanks NSF CAREER Award 1551943.

References

1 R. Que, Q. Shao, Q. Li, M. Shao, S. Cai, S. Wang and S. T. Lee, *Angew. Chem., Int. Ed.*, 2012, **51**, 5418–5422.
2 S. K. Singh, M. K. Singh, P. P. Kulkarni, V. K. Sonkar, J. J. A. Grácio and D. Dash, *ACS Nano*, 2012, **6**, 2731–2740.
3 J. T. Robinson, F. K. Perkins, E. S. Snow, Z. Wei and P. E. Sheehan, *Nano Lett.*, 2008, **8**, 3137–3140.
4 C. X. Guo, G. H. Guai and C. M. Li, *Adv. Energy Mater.*, 2011, **1**, 448–452.
5 C. Chung, Y. K. Kim, D. Shin, S. R. Ryoo, B. H. Hong and D. H. Min, *Acc. Chem. Res.*, 2013, **46**, 2211–2224.
6 M. Zhou, Y. Zhai and S. Dong, *Anal. Chem.*, 2009, **81**, 5603–5613.
7 N. R. Wilson, P. A. Pandey, R. Beanland, R. J. Young, I. A. Kinloch, L. Gong, Z. Liu, K. Suenaga, J. P. Rourke, S. J. York and J. Sloan, *ACS Nano*, 2009, **3**, 2547–2556.
8 K. P. Loh, Q. Bao, G. Eda and M. Chhowalla, *Nat. Chem.*, 2010, **2**, 1015–1024.
9 Y. Zhu, S. Murali, W. Cai, X. Li, J. W. Suk, J. R. Potts and R. S. Ruoff, *Adv. Mater.*, 2010, **22**, 3906–3924.
10 A. C. De Leon, B. J. Rodier, Q. Luo, C. M. Hemmingsen, P. Wei, K. Abbasi, R. Advincula and E. B. Pentzer, *ACS Nano*, 2017, **11**, 7485–7493.
11 D. C. Marcano, D. V. Kosynkin, J. M. Berlin, A. Sinitskii, Z. Z. Sun, A. Slesarev, L. B. Alemany, W. Lu and J. M. Tour, *ACS Nano*, 2010, **4**, 4806–4814.
12 J. Chen, B. Yao, C. Li and G. Shi, *Carbon*, 2013, **64**, 225–229.
13 S. Stankovich, D. A. Dikin, R. D. Piner, K. A. Kohlhaas, A. Kleinhammes, Y. Jia, Y. Wu, S. T. Nguyen and R. S. Ruoff, *Carbon*, 2007, **45**, 1558–1565.
14 X. Yang, Y. Tu, L. Li, S. Shang and X. M. Tao, *ACS Appl. Mater. Interfaces*, 2010, **2**, 1707–1713.
15 L. Graphene, M. a. Rafiee, J. Rafiee, Z. Wang, H. Song, Z. Yu and N. Koratkar, *ACS Nano*, 2009, **3**, 3884–3890.
16 J. D. Mangadlao, A. C. C. De Leon, M. J. L. Felipe, P. Cao, P. A. Advincula and R. C. Advincula, *ACS Appl. Mater. Interfaces*, 2015, **7**, 10266–10274.
17 A. Lerf, *Solid State Ionics*, 1997, **101–103**, 857–862.
18 G. Eda, G. Fanchini and M. Chhowalla, *Nat. Nanotechnol.*, 2008, **3**, 270–274.
19 O. C. Compton and S. T. Nguyen, *Small*, 2010, **6**, 711–723.
20 H. A. Becerril, J. Mao, Z. Liu, R. M. Stoltenberg, Z. Bao and Y. Chen, *ACS Nano*, 2008, **2**, 463–470.
21 S. Park, J. An, I. Jung, R. D. Piner, S. J. An, X. Li, A. Velamakanni and R. S. Ruoff, *Nano Lett.*, 2009, **9**, 1593–1597.
22 X. Sun, Z. Liu, K. Welsher, J. T. Robinson, A. Goodwin, S. Zaric and H. Dai, *Nano Res.*, 2008, **1**, 203–212.
23 S. Yongchao and T. Samulski Edward, *Nano Lett.*, 2008, **8**, 1679–1682.
24 G. Wang, B. Wang, J. Park, J. Yang, X. Shen and J. Yao, *Carbon*, 2009, **47**, 68–72.
25 S. Pei and H.-M. Cheng, *Carbon*, 2012, **50**, 3210–3228.
26 J. Zhang, H. Yang, G. Shen, P. Cheng, J. Zhang and S. Guo, *Chem. Commun.*, 2010, **46**, 1112–1114.
27 L. Lai, L. Chen, D. Zhan, L. Sun, J. Liu, S. H. Lim, C. K. Poh, Z. Shen and J. Lin, *Carbon*, 2011, **49**, 3250–3257.
28 S. Pei, J. Zhao, J. Du, W. Ren and H.-M. Cheng, *Carbon*, 2010, **48**, 4466–4474.
29 C. K. Chua and M. Pumera, *Chem. Soc. Rev.*, 2014, **43**, 291–312.
30 M. J. Fernández-Merino, L. Guardia, J. I. Paredes, S. Villar-Rodil, P. Solís-Fernández, A. Martínez-Alonso and J. M. D. Tascón, *J. Phys. Chem. C*, 2010, **114**, 6426–6432.

31 S. Stankovich, R. D. Piner, S. B. T. Nguyen and R. S. Ruoff, *Carbon*, 2006, **44**, 3342–3347.
32 A. C. De Leon, L. Alonso, J. D. Mangadlao, R. C. Advincula and E. Pentzer, *ACS Appl. Mater. Interfaces*, 2017, **9**, 14265–14272.
33 H. Bao, Y. Pan, Y. Ping, N. G. Sahoo, T. Wu, L. Li, J. Li and L. H. Gan, *Small*, 2011, **7**, 1569–1578.
34 D. C. Marcano, D. V. Kosynkin, J. M. Berlin, A. Sinitskii, Z. Sun, A. Slesarev, L. B. Alemany, W. Lu and J. M. Tour, *ACS Nano*, 2010, **4**, 4806–4814.
35 H. Yang, C. Shan, F. Li, D. Han, Q. Zhang and L. Niu, *Chem. Commun.*, 2009, 3880.
36 D. R. Dreyer, S. Park, C. W. Bielawski and R. S. Ruoff, *Chem. Soc. Rev.*, 2010, **39**, 228–240.
37 N. D. Luong, L. H. Sinh, L. S. Johansson, J. Campell and J. Seppala, *Chem.–Eur. J.*, 2015, **21**, 3183–3186.
38 P. Kanninen, N. D. Luong, L. H. Sinh, J. Flórez-Montaño, H. Jiang, E. Pastor, J. Seppälä and T. Kallio, *Electrochim. Acta*, 2017, **242**, 315–326.
39 C. Gómez-Navarro, R. T. Weitz, A. M. Bittner, M. Scolari, A. Mews, M. Burghard and K. Kern, *Nano Lett.*, 2007, **7**, 3499–3503.
40 Z. Wei, D. Wang, S. Kim, S.-Y. Kim, Y. Hu, M. K. Yakes, A. R. Laracuente, Z. Dai, S. R. Marder, C. Berger, W. P. King, W. A. de Heer, P. E. Sheehan and E. Riedo, *Science (80-)*, 2010, **328**, 1373–1376.
41 J. D. Mangadlao, C. M. Santos, M. J. L. Felipe, A. C. C. de Leon, D. F. Rodrigues and R. C. Advincula, *Chem. Commun.*, 2015, **51**, 2886–2889.
42 D. Yang, A. Velamakanni, G. Bozoklu, S. Park, M. Stoller, R. D. Piner, S. Stankovich, I. Jung, D. A. Field, C. A. Ventrice and R. S. Ruoff, *Carbon*, 2009, **47**, 145–152.
43 S. Park, J. An, J. R. Potts, A. Velamakanni, S. Murali and R. S. Ruoff, *Carbon*, 2011, **49**, 3019–3023.
44 K. Krishnamoorthy, M. Veerapandian, K. Yun and S. J. Kim, *Carbon*, 2013, **53**, 38–49.
45 Z. Wang, Y. Dong, H. Li, Z. Zhao, H. Bin Wu, C. Hao, S. Liu, J. Qiu and X. W. D. Lou, *Nat. Commun.*, 2014, **5**, 1–8.
46 L. Zhang, L. Ji, P.-A. Glans, Y. Zhang, J. Zhu and J. Guo, *Phys. Chem. Chem. Phys.*, 2012, **14**, 13670.
47 G. Gonçalves, P. A. A. P. Marques, A. Barros-Timmons, I. Bdkin, M. K. Singh, N. Emami and J. Grácio, *J. Mater. Chem.*, 2010, **20**, 9927.
48 C. K. Chua and M. Pumera, *Chem.–Eur. J.*, 2013, **19**, 2005–2011.
49 R. N. Wenzel, *Ind. Eng. Chem.*, 1936, **28**, 988–994.
50 Y. Zhu, S. H. Lee, D. R. Dreyer, J. An, A. Velamakanni, D. Piner, S. Park, Y. Zhu, S. O. Kim, C. W. Bielawski and R. S. Ruoff, *Macromol. Rapid Commun.*, 2009, **31**, 281–288.
51 H. Kim, A. A. Abdala and C. W. MacOsko, *Macromolecules*, 2010, **43**, 6515–6530.
52 A. Dimiev, *Science (80-)*, 2011, **1168**, 1168–1172.
53 M. Moniruzzaman and K. I. Winey, *Macromolecules*, 2006, **39**, 5194–5205.
54 J. Ding, M. Wang, X. Zhang, C. Ran, J. Shao and Y. Ding, *Appl. Phys. Lett.*, 2014, **105**, 233106.
55 A. Dimieve and J. Tour, *ACS Nano*, 2014, **8**, 3060–3068.
56 M. M. Gudarzi and F. Sharif, *Soft Matter*, 2011, **7**, 3432.
57 A. B. Lowe, *Polym. Chem.*, 2010, **1**, 17–36.
58 J. Shang, L. Ma, J. Li, W. Ai, T. Yu and G. G. Gurzadyan, *Sci. Rep.*, 2012, **2**, 792.
59 S. J. Leigh, R. J. Bradley, C. P. Purssell, D. R. Billson and D. A. Hutchins, *PLoS One*, 2012, **7**, 1–6.
60 J. Zhang, H. Yang, G. Shen, P. Cheng, J. Zhang and S. Guo, *Chem. Commun.*, 2010, **46**, 1112–1114.
61 I. Jung, D. A. Dikin, R. D. Piner and R. S. Ruoff, *Nano Lett.*, 2008, **8**, 4283–4287.